Journal of
Synchrotron
Radiation

ISSN 0909-0495

Received 21 September 2010
Accepted 9 December 2010

Densification of sol–gel silica thin films induced by hard X-rays generated by synchrotron radiation

Plinio Innocenzi,[a]* Luca Malfatti,[a] Tongjit Kidchob,[a] Stefano Costacurta,[b] Paolo Falcaro,[c] Benedetta Marmiroli,[d] Fernando Cacho-Nerin[d] and Heinz Amenitsch[d]

[a]Laboratorio di Scienza dei Materiali e Nanotecnologie, University of Sassari and CR-INSTM, Palazzo del Pou Salit, Piazza Duomo 6, 07041 Alghero (Sassari), Italy, [b]Associazione CIVEN, Via delle Industrie 5, 30175 Venezia, Italy, [c]Division of Materials Science and Engineering, CSIRO, Private Bag 33, Clayton South MDC, Victoria 3169, Australia, and [d]Institute of Biophysics and Nanosystems Structure Research, Austrian Academy of Sciences, Schmiedlstrasse 6, 8042 Graz, Austria. E-mail: plinio@uniss.it

In this article the effects induced by exposure of sol–gel thin films to hard X-rays have been studied. Thin films of silica and hybrid organic–inorganic silica have been prepared *via* dip-coating and the materials were exposed immediately after preparation to an intense source of light of several keV generated by a synchrotron source. The samples were exposed to increasing doses and the effects of the radiation have been evaluated by Fourier transform infrared spectroscopy, spectroscopic ellipsometry and atomic force microscopy. The X-ray beam induces a significant densification on the silica films without producing any degradation such as cracks, flaws or delamination at the interface. The densification is accompanied by a decrease in thickness and an increase in refractive index both in the pure silica and in the hybrid films. The effect on the hybrid material is to induce densification through reaction of silanol groups but also removal of the organic groups, which are covalently bonded to silicon *via* Si—C bonds. At the highest exposure dose the removal of the organic groups is complete and the film becomes pure silica. Hard X-rays can be used as an efficient and direct writing tool to pattern coating layers of different types of compositions.

© 2011 International Union of Crystallography
Printed in Singapore – all rights reserved

Keywords: sol–gel; deep X-ray lithography; thin films.

1. Introduction

Sol–gel processing allows oxide and hybrid organic–inorganic materials to be prepared through a soft chemistry route starting from low temperatures. The solid-state material is finally obtained *via* condensation reactions that are governed by the chemistry of the solution and the processing conditions. Sol–gel processing is widely used for fabrication of functional films and is also the basis for the development of different kinds of self-assembled nanomaterials (Soler-Illia & Innocenzi, 2006). The deposition of the films is carried out under controlled conditions of atmosphere, temperature and relative humidity generally *via* spin-coating or dip-coating. Immediately after the deposition the films are largely uncondensed and maintain a gel-like state (xerogel) until they are further processed. Condensation is finally achieved after a drying step at low temperatures, generally around 323–353 K, and firing at higher temperatures. The densification of the material is realised *via* polycondensation reactions through the MOH species (M = metal or metalloid) while the firing temperature governs the final density.

On the other hand, beside a thermal treatment, densification can be achieved using external sources of energy. A known example is given by the action of UV light which has been used for photo-annealing of thin sol–gel films (Van de Leest, 1995; Bohannan *et al.*, 2002); antireflective coatings on cathode ray tubes have been produced by UV annealing of silica–titania sol–gel films. Selective UV irradiation of acetylacetonate modified alkoxide precursors has also been applied to obtain patterned zirconia and titania films (Kintaka *et al.*, 2000). In general, sol–gel films have shown to be sensitive to UV exposure (Ma *et al.*, 2001; Innocenzi & Brusatin, 2004; Lasagni *et al.*, 2005), laser light (Lasagni *et al.*, 2005) and X-ray irradiation (Brusatin *et al.*, 2008), and different photolithographic technologies which are based on the direct interaction of the light with the material have been developed so far. The details of the processes induced by irradiation of the sol–gel material by different light sources and energies have not yet

been studied and understood in detail; secondary electrons generated from the film substrates (Kruk *et al.*, 2000) as far as the formation of radical species upon light illumination are possible causes (Werst & Vinokur, 2001). On the other hand, the UV (Fan *et al.*, 2000; Seward *et al.*, 1997) induced densification of silica glass is a well known phenomenon.

We have recently used hard X-ray radiation as a writing tool on different materials to produce complex patterns and structures. Hard X-rays are traditionally used for deep X-ray lithography (DXRL) in a process called LIGA, from the German LIthographie Galvanoformung Abformung (electroforming moulding lithography), and is applied for producing high-precision materials for micromechanics (Mappes *et al.*, 2007; Romanato *et al.*, 2004). High-aspect-ratio materials can be easily obtained on the microscale even if DXRL potential application can be extended to a submicrometer scale (Ehrfeld *et al.*, 1999; Meyer *et al.*, 2008). Another advantage of DXRL is that the lithography is not limited to two-dimensional structures, but complex three-dimensional shape materials (Katoh *et al.*, 2001) such as optical components, micromechanical devices (Chung *et al.*, 2000) and photonic crystals (Feiertag *et al.*, 1997; Katsarakis *et al.*, 2002) can also be fabricated. We have already demonstrated that the effect of hard X-rays on coating layers can be used to produce patterns in mesoporous (Falcaro *et al.*, 2008, 2009*a*), sol–gel (Falcaro *et al.*, 2009*b*; Falcaro & Innocenzi, 2010), PE-CVD (Costacurta *et al.*, 2010) and soft matter films (Innocenzi *et al.*, 2010) and to generate *in situ* metallic nanoparticles (Malfatti *et al.*, 2010) in patterned structures. In particular, to obtain a degree of densification of silica in sol–gel films such as that obtained upon exposure to hard X-rays is difficult using UV or soft X-rays; high condensation can be obtained in a short time, at least in comparison with thermal or UV annealing. If we apply intense sources of X-rays to promote densification it is even possible to obtain a direct patterning of the films. If the sol–gel films are immediately exposed to hard X-rays when they are still in a soft-like state (xerogel), densification of the exposed part is achieved in a few minutes. It is therefore possible simply by washing the film with ethanol to remove the unexposed part which does not significantly condense in this short time interval.

The potentialities of the technique appear still to be fully exploited and the effect of hard X-rays on soft and solid-state matter still to be fully studied and understood. In this article we have used thin sol–gel silica films, either purely inorganic or hybrid organic–inorganic, to study the effect of exposure to high-energy radiation of materials that are only partially condensed. The purpose of the work is to give a better insight into the basic chemical–physical effects of hard X-ray interaction with oxides and hybrid organic–inorganic sol–gel materials when they are still in a 'soft' state to allow future technological developments based on these phenomena.

2. Experimental

Tetraethoxysilane (TEOS), methyltriethoxysilane (MTES), 1 *M* hydrochloric acid (HCl) and ethanol (EtOH) were purchased from Sigma Aldrich and used as received. P-type boron-doped silicon wafers were employed as the substrates. A silica precursor sol (called 'T') was prepared by mixing 21 cm^3 EtOH, 4.4 cm^3 TEOS, 1 cm^3 H_2O and 0.5 cm^3 HCl 1 *M*. The sol was stirred for 2 h and deposited by dip coating (20% relative humidity at 298 K) on Si wafers; the withdrawal speed was set at 300 mm s^{-1}. Another sol (called 'M') was prepared in a similar way, but TEOS was substituted by an equimolar amount of TEOS + MTES in the molar ratio 2:1, which corresponds to 2.93 cm^3 TEOS and 1.33 cm^3 MTES.

The films were directly exposed to hard X-rays using the DXRL beamline at the Elettra synchrotron facility (Trieste, Italy). The films were irradiated with different doses (in this case expressed as energy per unit area incident at the sample surface) by changing the exposure time. The films were exposed to increasing doses, 94, 188, 377, 754, 1508 and 3015 J cm^{-2}, which corresponded to an average irradiation time of 10 to 400 s. The sample was mounted on the top of a water-cooled stainless steel plate (scanner) which was continuously rastering the sample to allow a homogeneous exposure of areas larger than the beam size; the scanner rate was set to 20 mm s^{-1}. At the exposure plane (position of the sample) the beam size was 115.5 mm × 10.6 mm. Under these conditions the T and the M coatings were exposed to increasing energies.

The beamline layout is shown in Fig. 1. The vertical size of the bending-magnet source point is 43 µm for a root-mean-square (r.m.s.) vertical divergence of less then 15 µrad. The features of the bending magnet are carefully described by Pérennès and co-workers (Pérennès *et al.*, 2001). A 200 µm-thick beryllium window separates the ultra-high-vacuum part of the front-end from the high-vacuum external beamline part. A second Be window of the same thickness divides the high-vacuum area from the working chamber area. The distance between the source and the scanning stage is 20.8 m. During the exposure process the working chamber is filled with He

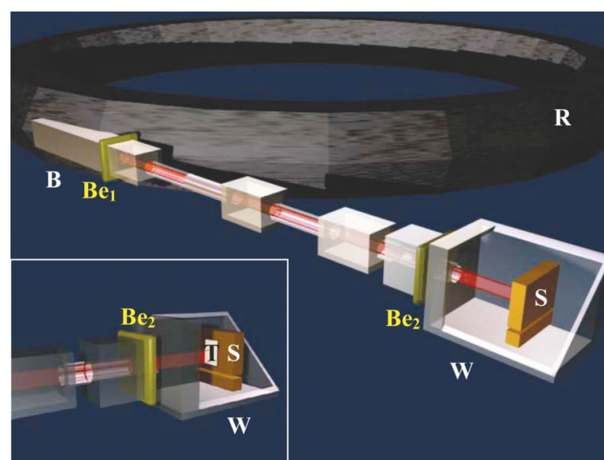

Figure 1
Layout of the DXRL beamline at Elettra (R, synchrotron ring; B, bending magnet; Be_1 and Be_2, beryllium windows; W, section of the working chamber; S, scanner; T, sample). The height/width ratio of the beam at the exposure plane is 10.8.

(100 mbar) for cooling the mask/substrate system and decreasing the ozone formation.

Fourier transform infrared measurements were performed using a Vertex 70V Bruker spectrometer in the 375–4000 cm^{-1} range with a resolution of 4 cm^{-1}. A RT-DTGS detector and a KBr beam splitter were used. The baseline was corrected using a concave rubber-band method (*OPUS 6.5* software) using 64 baseline points and two iterations.

The film thickness and refractive index were measured using an α-SE Wollam spectroscopic ellipsometer; the film optical properties were fitted using a Cauchy model for non-absorbing materials.

Atomic force microscopy was used to analyze the surface of the films using a NT-MDT Ntegra AFM in non-contact mode. The surface morphology was evaluated at a scan speed of 0.5 Hz in semi-contact mode, using a high-aspect-ratio silicon tip with nominal resonance frequency of 150 kHz, 5.5 N m^{-1} force constant, and 10 nm typical curvature radius.

Simulation of the photon transmittance as a function of incident photon energy (eV) for a silica dense film has been performed using the 'X-ray Interaction with Matter Tool' available online at http://www-cxro.lbl.gov/.

3. Results and discussion

We have used FTIR absorption spectroscopy in combination with spectroscopic ellipsometry to evaluate the effect on the sol–gel films of X-ray exposure. We have compared the FTIR spectra, refractive index and thickness of films deposited under the same processing conditions, *i.e.* the same relative humidity, temperature and withdrawal speed, but exposed to different X-ray energies. We have carefully monitored the elapsed time between the deposition of the films and their exposure to avoid the possibility that the aging of the material could affect the experimental results.

3.1. Effect of X-ray exposure on sol–gel silica film

The effect of radiation has been evaluated by comparing the change induced by X-ray exposure with an as-deposited sol–gel film. The FTIR absorption spectra in the 1275–850 cm^{-1} range of as-deposited silica films exposed to different X-ray doses are shown in Fig. 2. This wavenumber interval corresponds to the region of Si—O—Si antisymmetric stretching, ν_{as}(Si—O—Si) (1250–1000 cm^{-1}) and Si—OH stretching (1000–850 cm^{-1}) in silica materials (Innocenzi, 2003). The main band of strongest intensity peaking around 1050 cm^{-1} is assigned to the silica stretching mode; this band is accompanied by a typical intense shoulder at higher wavenumbers (1100–1250 cm^{-1}). This infrared region is generally taken as a reference to evaluate the condensation of silica species, especially in the case of silica sol–gel materials (Almeida, 1992).

With an increase in condensation, the bands in this region undergo a significant change that allows the effect of external processing conditions (such as thermal treatment or aging) on the material structure to be identified. The densification of

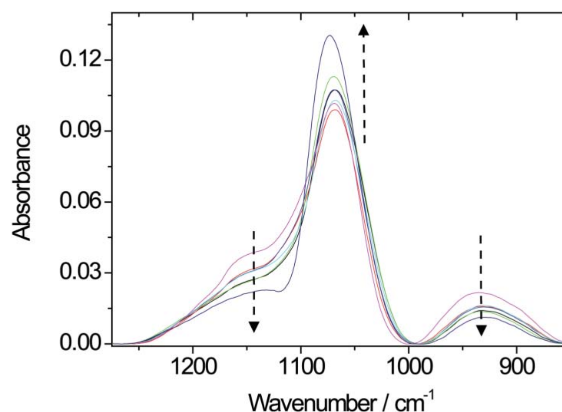

Figure 2
FTIR absorption spectra in the 1275–850 cm^{-1} range of silica films exposed to different X-ray doses. The arrows in the figure show the directions of change in intensity with the increase of dose; at higher doses the Si—OH band at 930 cm^{-1} and the shoulder at 1150 cm^{-1} decrease, while the Si—O—Si band at 1070 cm^{-1} increases in intensity. Colours of the curves: magenta, as-deposited (unexposed reference sample); red, 94 J cm^{-2}; cyan, 188 J cm^{-2}; blue, 377 J cm^{-2}; black, 754 J cm^{-2}; green, 1508 J cm^{-2}; navy, 3015 J cm^{-2}.

silica films is due to condensation reactions of silanols which produce a more interconnected silica network. This effect, whatever the external cause (radiation or thermal), is clearly recorded by the silica spectra that show several changes: reduction in intensity of the silanols stretching band (around 950 cm^{-1}); increase in intensity of the ν_{as}(Si—O—Si) band; shift of the ν_{as}(Si—O—Si) band to higher wavenumbers; change in the full width at half-maximum of the ν_{as}(Si—O—Si) band [TO_3 (TO = transverse optical) mode] and finally the decrease of the shoulder at 1250 cm^{-1}. In particular, the 1250 cm^{-1} wide shoulder, which is assigned either to a broadened signature of the longitudinal optical (LO) component of the TO_3 antisymmetric stretching or to a mixed LO–TO mode with dominant LO character, has a particular importance in sol–gel materials, especially in thin films. This shoulder increases in intensity with an increase of the porosity because of the IR radiation within the pores and the consequent activation of the LO modes (Galeener & Lucovsky, 1976; Innocenzi *et al.*, 2003; Almeida, 1992; Malfatti *et al.*, 2007). FTIR appears, therefore, very effective for investigating silica materials, such as sol–gel silica-based films, which at the first processing stage show only a low degree of condensation. Furthermore, sol–gel films after the deposition are in the so-called *xerogel* phase, which represents a peculiar state of the material during which the network is only partially formed and a liquid phase is still present. If, during film deposition, the evaporation of ethanol is very fast, water remains in the film for a longer time and, at room temperature, several hours are necessary to observe a significant evaporation of residual water.

We have, therefore, exposed the sol–gel films in the *xerogel* state and observed the effect of X-ray exposure by FTIR. The silica spectra in Fig. 2 show that by increasing the X-ray dose a higher degree of silica condensation is produced, as pointed out by the systematic change of the spectra according to

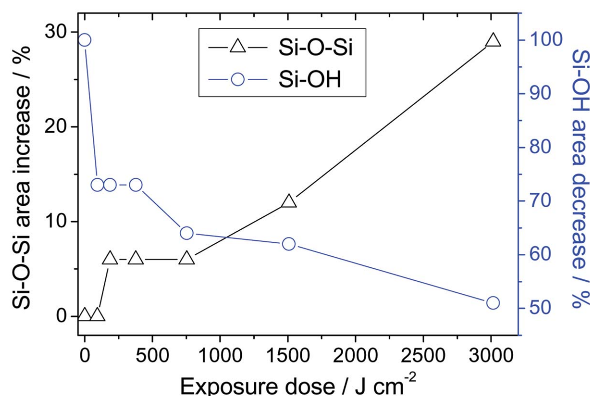

Figure 3
Relative change of the integrated areas of the ν_{as}(Si—O—Si) band (left axis) and Si—OH band (right axis) as a function of the exposure dose in silica sol–gel films. The lines are a visual guide only.

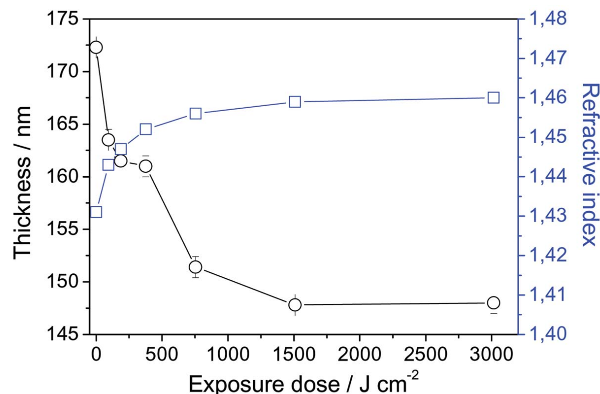

Figure 4
Variation of thickness (left axis) and refractive index (right axis) as a function of the exposure dose for a silica film. The lines are a visual guide only.

condensation conditions. The arrows in Fig. 2 show the directions of change in intensity of the different absorption bands with the increase of dose; at higher doses the Si—OH band at 930 cm^{-1} and the shoulder at 1150 cm^{-1} decrease while the Si—O—Si band at 1070 cm^{-1} increases.

To find a more quantitative and direct indication of the degree of condensation induced by X-rays we have integrated the areas of Si—OH and ν_{as}(Si—O—Si) (including the shoulder at higher wavenumbers) in the different spectra. The results of the integration are reported in Fig. 3, which shows the relative change of the integrated areas as a function of the energy on the sample. We can observe that the densification of silica increases with an increase of the exposure dose. A 50% decrease in the Si—OH band is accompanied by an increase of 30% of the Si—O—Si band which indicates that a significant condensation is induced upon X-ray exposure. The difference in the relative change is due to the fact that we have integrated the Si—O—Si band in the full range which includes contributions from different silica vibrational modes. We have preferred to integrate the whole band rather than using deconvoluted curves to avoid an arbitrary choice of components that in this range are quite difficult to separate [see Innocenzi (2003) for a detailed discussion]. We have also to account for the fact that the beamline is working at low pressure (100 mbar) in a helium atmosphere; the effect of a vacuum on the densification of the film has also in principle to be considered. By making *in situ* FTIR measurements on as-deposited films we have verified that an effect of this type is observed only at much lower pressure (Malfatti *et al.*, 2007) than that used in the vacuum chamber of the beamline.

We have also observed by spectroscopic ellipsometry the effect of radiation exposure on film thickness and refractive index. Fig. 4 shows the changes in thickness and refractive index as a function of exposure dose. The trend is similar to that observed in FTIR spectra: higher doses produce an enhanced shrinkage and increase in refractive index. The shrinkage of the silica sol–gel film is a typical effect induced by condensation and is reflected in an increase in the refractive index. The films after X-ray exposure even at the highest dose do not show any crack or specific defect on the surface. An important result is therefore that exposure of the materials to high-energy light induces densification without damage of the sol–gel film.

3.2. Effect of X-ray exposure on sol–gel methyl modified hybrid silica films

We have also evaluated the effect of the X-ray irradiation on sol–gel hybrid silica films. A hybrid material sample, which has been prepared by co-condensation of methyltriethoxysilane, as the source of methyl groups covalently bonded to the silica network and tetraethylortosilicate, has been exposed to increasing doses of radiation to evaluate the effects of X-rays. Fig. 5 shows the infrared absorption spectra in the 1250–950 cm^{-1} wavenumber range as a function of exposure dose. In this range the FTIR spectra of the hybrid films are the same as pure silica (Fig. 2), with the exception of an additional band peaking at around 1090 cm^{-1} observed only in the freshly deposited films. Higher X-ray doses produce an increase in intensity of the ν_{as}(Si—O—Si) band accompanied by a reduction of the higher-wavenumbers shoulder, as shown by the arrow in Fig. 5(*a*). The presence of the band owing to unhydrolyzed ethoxy moieties (–OCH_2CH_3) at 1090 cm^{-1} indicates that the as-deposited hybrid films are less condensed with respect to the pure silica sol–gel films, at least at the early processing stage. After exposure to 94 J cm^{-2} the 1090 cm^{-1} band disappears indicating that densification, even at the lowest experimental dose, is induced in the film. Radiation effects on alkoxy and siloxy ligands bonded to silica have already been reported in the literature (Kruk *et al.*, 2000) and it has been shown that several mechanisms are responsible for the dissociation of the ligand and then densification of the species. The same mechanisms operate in the present case, when the material at the early processing stage is largely uncondensed and shows still the presence of unreacted alkoxy species. For a better visualization of the FTIR results we have also shown the spectra using a three-scales representation (that for simplicity we indicate as three-dimensional spectra). Fig. 5(*b*) shows the three-dimensional spectra. The *x*-axis represents the wavenumber, the *y*-axis the dose scale in J cm^{-2}

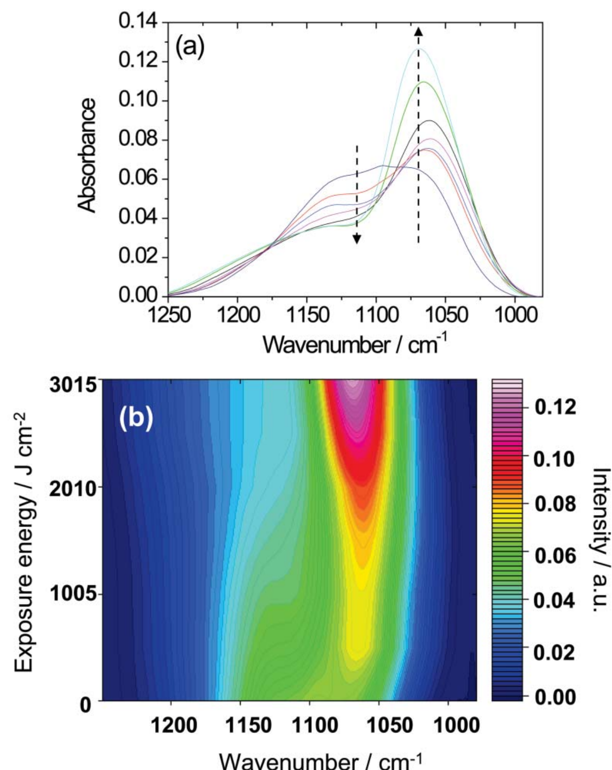

Figure 5
(a) FTIR absorption spectra of hybrid silica films (MTES-TEOS) in the 1250–950 cm^{-1} wavenumber range as a function of dose; the arrows indicate the change in intensity of the bands with the increase of the dose. At higher doses the Si—O—Si band at 1070 cm^{-1} increases in intensity while the shoulder at 1150 cm^{-1} decreases. Colours of the curves: magenta, as-deposited (unexposed reference sample); red, 94 J cm^{-2}; cyan, 188 J cm^{-2}; blue, 377 J cm^{-2}; black, 754 J cm^{-2}; green, 1508 J cm^{-2}; navy, 3015 J cm^{-2}. (b) Contour representation of the data in (a). The x-axis represents the wavenumber and the y-axis the dose scale in seconds. The colour scale corresponds to absorbance.

and the different colours the intensity scale of absorbance. Fig. 5(b) clearly shows the increase in intensity of the silica stretching band: the decrease of the shoulder intensity indicates the proceeding of the condensation reactions with increasing exposure doses. We have carried out a semi-quantitative evaluation of the increase of the silica condensation by integrating the ν_{as}(Si—O—Si) band including the shoulder at higher wavenumbers. Fig. 6 shows the change (%) calculated with respect to the as-deposited film of the integrated band area as a function of the dose. The results indicate that the process of densification is significantly enhanced at higher doses and that at 400 s of exposure an increase of 89% of the silica band area is observed. In the case of hybrid samples the radiation should, however, affect not only the condensation process but also the Si—C, C—C and C—H bonds. We have, in fact, observed that the infrared signals assigned to these species significantly change with exposure to X-rays. We have used as reference the Si—CH_3 band at 1275 cm^{-1} whose changes as a function of exposure dose are shown in Fig. 7(a). We observe a continuous decrease in intensity of the band with an increase of the dose up to 3015 J cm^{-2}; at this dose the methyl groups are completely removed from the sample. We have integrated the area of the bands in Fig. 7(b) and reported

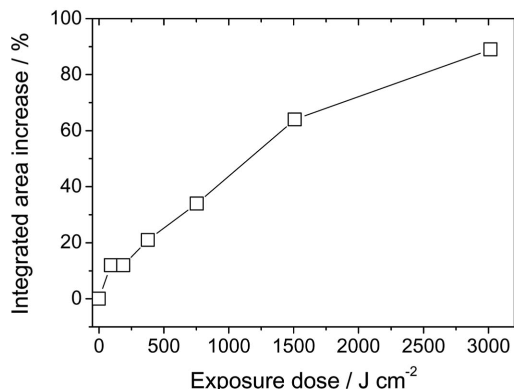

Figure 6
Variation of the integrated area of the Si—O—Si antisymmetric stretching band (1250–980 cm^{-1}) of silica hybrid films (MTES-TEOS) as a function of the X-rays exposure dose. The line is a visual guide only.

the change (area % variation) as a function of the dose. It is also important to note that after using a dose of 3015 J cm^{-2} no infrared signal owing to organic species could be observed, which indicates that all the organic moieties covalently bonded to Si are removed by scissions of bonds induced by X-rays and no organic fragments remain entrapped in the samples.

The effect of X-rays on the thickness and refractive index of the film exposure is shown in Fig. 8. It is important to observe that the X-ray exposure of a hybrid film has a double effect,

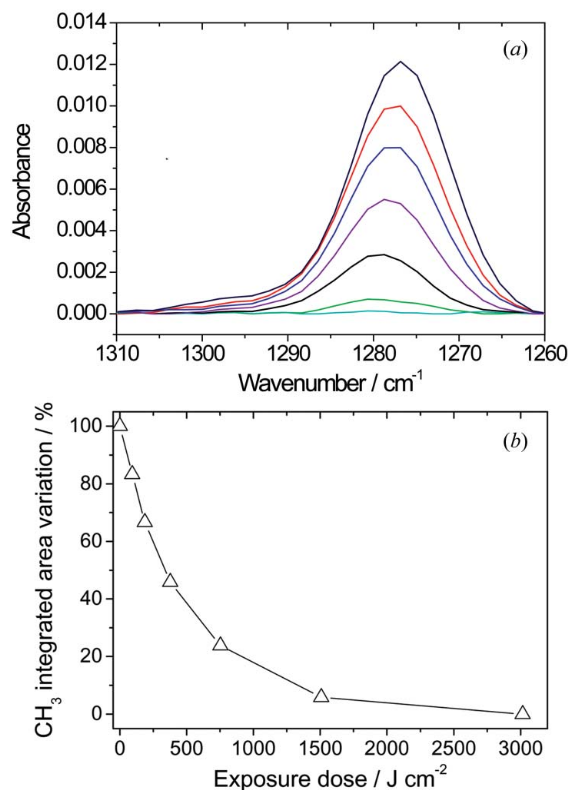

Figure 7
(a) FTIR absorption spectra of a MTES-TEOS hybrid film in the 1310–1260 cm^{-1} range upon exposure to increasing doses of radiation. (b) Change of the integrated area (%) as a function of dose. The line is a visual guide only.

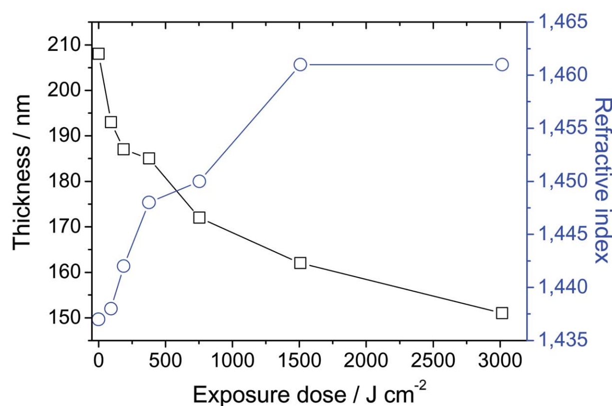

Figure 8
Variation of thickness (left axis) and refractive index (right axis) as a function of the dose for an MTES-TEOS hybrid film. The lines are a visual guide only.

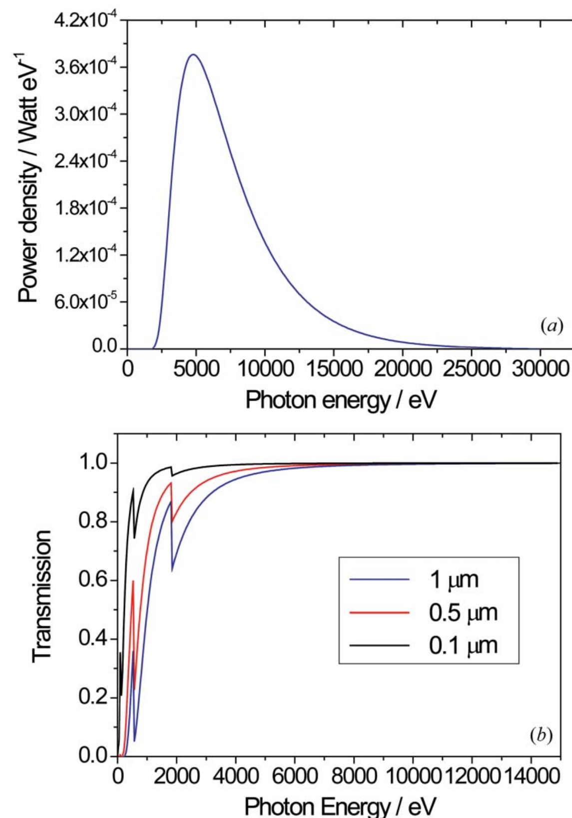

Figure 9
(*a*) Power density spectrum of synchrotron light at the Elettra Deep X-ray Lithography beamline. (*b*) Normalized transmittance of photons as a function of incident photon energy (eV) calculated for a silica dense film of thickness 0.1 µm (black line), 0.5 µm (red line) and 1 µm (blue line).

densification and removal of the organic functions. At the end of the X-ray processing we obtain a purely inorganic material. In fact, if we compare the refractive index of the pure silica and hybrid organic–inorganic films after exposure to the highest dose we observe that it is the same, $n = 1.46$, which is an indication that at the end of the process we obtain a pure silica material of similar degree of condensation. The densification effect is independent of the aging time of the precursor sol; in fact, we have observed a similar trend both for pure silica and hybrid silica films obtained from fresh and ten-day-old sols (results not shown).

The experimental data show, therefore, that exposure to hard X-rays of silica and hybrid silica films prepared *via* sol–gel processing produces a densification of the material, whose extent depends on the exposure dose.

We have observed the surface morphology by atomic force microscopy and we have found that the surface remains homogeneous even after exposure to the highest dose, and the average surface roughness, which is in the 10–15 nm range, did not change for the different samples. This value is higher with respect to thermal processed films and is likely to be due to X-ray processing but we have seen a reduction of roughness after a post-processing thermal treatment. On the other hand the X-ray exposure has caused neither surface damage nor cracking during densification of the sample.

3.3. Densification mechanisms

The power density spectrum of X-ray synchrotron light at the Elettra Deep X-ray Lithography beamline is reported in Fig. 9(*a*) (Malfatti *et al.*, 2010). The photons that are used to irradiate the silica sol–gel films have an energy between 2500 and 12000 eV, which is a much higher range of energies in comparison with those typically used in soft lithography (0.5–2 keV). The advantage of using high-energy photons is the higher penetration depth and therefore the possibility to obtain high-aspect-ratio microstructures in thick films by X-ray lithography (Ehrfeld *et al.*, 1999; Meyer *et al.*, 2008). If we define the dose contrast as the ratio between the energy per unit area incident at the surface and that at the bottom of the film, a value close to unity indicates a uniform dose distribution in the film depth, and implies that most of the irradiation power has also penetrated the material. The penetration depth of X-rays is directly related to the absorption coefficient of the material, which is a function of wavelength (Cheng *et al.*, 1997). We have calculated the theoretical transmission as a function of photon energy in eV for a silica dense film (2.2 g cm^{-3} density) of different thickness. The calculated transmission *versus* photon energy plots of a film of 0.1 µm (black line), 0.5 µm (red line) and 1 µm (blue line) µm thickness is shown in Fig. 9(*b*). In general, the thicker the film, the higher the absorption of the low-energy photons; the high-energy photons of DXRL have, therefore, a higher penetration depth, allowing a dose contrast closer to unity and a more uniform irradiation along the film depth. This approximation is made for silica dense films while the experimentally used materials are uncondensed silica and hybrid films. The thickness of the films that have been exposed to the high-energy photons is smaller than 0.5 µm and therefore the dose contrast can be considered to be unity. It is also important to note that the photoelectrons generated by the silicon substrate do not cause any delamination or adhesion loss at the film–substrate interface; even at the higher radiation doses both the silica and hybrid films remain always well adherent to the substrate. The direct exposure of silica does not also create the typical

phenomenon of bubbling that is observed at high doses in polymethylmethacrylate (PMMA) which is a severe limitation in application of DXRL to polymeric materials. On the other hand, detailed discussion of the mechanism of densification is, however, quite complex; the physical–chemical effects of radiation exposure, which include electron, X-ray, UV light and γ-ray radiation during the different steps of processing of inorganic and hybrid materials, are only partially studied. In our work we have observed that the exposure to hard X-rays induces densification of Si—OH and $Si—OC_2H_5$ species, which can be attributed to the formation of free radicals (Innocenzi, 2003). The second effect is the removal of organic molecules that are bound to silicon *via* the covalent Si—C bond, which is also likely to be caused by free radicals generated by X-rays; we can also exclude the dissociation of the Si—O—Si bond by X-rays because the infrared spectra do not show any evidence of decrease of silica bands with X-ray exposure but only indicate densification as the main effect produced by the high-energy light.

4. Conclusions

Sol–gel silica and hybrid organic–inorganic silica films have been exposed to increasing doses of hard X-rays to study the effect of radiation on the material. We have observed that the exposure of as-deposited fresh films, whose network is still largely uncondensed, produces a significant densification of the silica network. In the hybrid films the X-ray exposure removes the organic functional groups besides inducing condensation of silica. The extent of condensation induced by X-rays depends on the dose; higher doses produce a larger condensation. The exposure to X-rays does not form any crack or defect on the films and at the same time the coatings remain well adherent to the substrate.

The results show that the direct application of intense sources of X-rays can be used as an efficient lithographic tool for oxides and hybrid films.

We acknowledge travel funding provided by the International Synchrotron Access Program (ISAP) managed by the Australian Synchrotron. The ISAP is an initiative of the Australian Government being conducted as part of the National Collaborative Research Infrastructure Strategy. Benedetta Marmiroli and Fernando Cacho-Nerin acknowledge the financial support from the EU project SAXIER, contract no. RIDS 011934.

References

Almeida, R. M. (1992). *Phys. Rev. B*, **45**, 161–170.
Bohannan, E. W., Gao, X. R., Gaston, K. R., Doss, C. D., Sotiriou-Leventis, C. & Leventis, N. (2002). *J. Sol–Gel Sci. Techn.* **23**, 235–245.
Brusatin, G., Della Giustina, G., Romanato, F. & Guglielmi, M. (2008). *Nanotechnology*, **19**, 175306.
Cheng, Y., Kuo, N.-Y. & Su, H. (1997). *Rev. Sci. Instrum.* **68**, 2163–2166.
Chung, S. J., Hein, H., Hirata, T., Mohr, J. & Akashi, T. (2000). *Microsyst. Technol.* **6**, 149–153.
Costacurta, S., Malfatti, L., Patelli, A., Amenitsch, H., Marmiroli, B., Falcaro, P. & Innocenzi, P. (2010). *Plasma Proc. Polym.* **7**, 459–466.
Ehrfeld, W., Hessel, V., Löwe, H., Schulz, C. & Weber, L. (1999). *Microsyst. Technol.* **5**, 105–122.
Falcaro, P., Costacurta, S., Malfatti, L., Kidchob, T., Takahashi, M., Casula, M., Piccinini, M., Marcelli, A., Marmiroli, B., Amenitsch, H., Schiavuta, P. & Innocenzi, P. (2008). *Adv. Mater.* **20**, 1864–1869.
Falcaro, P. & Innocenzi, P. (2010). *J. Sol–Gel Sci. Technol.* doi:10.1007/s10971-009-2127-7.
Falcaro, P., Malfatti, L., Kidchob, T., Giannini, G., Falqui, A., Casula, M. F., Amenitsch, H., Marmiroli, B., Grenci, G. & Innocenzi, P. (2009*a*). *Chem. Mater.* **21**, 2055–2061.
Falcaro, P., Malfatti, L., Vaccari, L., Amenitsch, H., Marmiroli, B., Grenci, G. & Innocenzi, P. (2009*b*). *Adv. Mater.* **21**, 4932–4936.
Fan, P. A., Oldham, W. G. & Haller, E. E. (2000). *J. Appl. Phys.* **87**, 3287–3293.
Feiertag, G., Ehrfeld, W., Freimuth, H., Kolle, H., Lehr, H., Schmidt, M., Sigalas, M. M., Soukoulis, C. M., Kiriakidis, G. & Pedersen, T. (1997). *Appl. Phys. Lett.* **71**, 1441–1443.
Galeener, F. L. & Lucovsky, G. (1976). *Phys. Rev. Lett.* **37**, 1474–1478.
Innocenzi, P. (2003). *J. Non-Cryst. Solids*, **316**, 309–319.
Innocenzi, P. & Brusatin, G. (2004). *J. Non-Cryst. Solids*, **333**, 137–142.
Innocenzi, P., Falcaro, P., Grosso, D. & Babonneau, F. (2003). *J. Phys. Chem. B*, **107**, 4711–4717.
Innocenzi, P., Kidchob, T., Costacurta, S., Falcaro, P., Cacho-Nerin, F., Marmiroli, B. & Amenitsch, H. (2010). *Soft Matter*, **6**, 3172–3176.
Katoh, T., Nishi, N., Fukugawa, M., Ueno, H. & Sugiyama, S. (2001). *Sens. Actuators A*, **89**, 10–15.
Katsarakis, M., Bender, M., Singleton, L., Kiriakidis, G. & Soukoulis, C. M. (2002). *Microsyst. Technol.* **8**, 74–77.
Kintaka, K., Nishii, J. & Tohge, N. (2000). *Appl. Opt.* **39**, 489–493.
Kruk, M., Jaroniec, M., Sakamoto, Y., Terasaki, O., Ryoo, R. & Ko, H. (2000). *J. Phys. Chem. B*, **104**, 292–301.
Lasagni, A. S., Seyler, M., Holzapfel, C., Maier, W. F. & Mucklich, F. (2005). *Adv. Mater.* **17**, 2228–2232.
Ma, J. H., Wu, G. M., Shen, J. & Wang, J. (2001). *J. Inorg. Mater*, **16**, 1174–1180.
Malfatti, L., Kidchob, T., Falcaro, P., Costacurta, S., Piccinini, M., Cestelli Guidi, M., Marcelli, C., Corrias, A., Casula, M., Amenitsch, H. & Innocenzi, P. (2007). *Microp. Mesop. Mater.* **103**, 113–120.
Malfatti, L., Marongiu, D., Costacurta, S., Falcaro, P., Amenitsch, H., Marmiroli, B., Grenci, G., Casula, M. & Innocenzi, P. (2010). *Chem. Mater.* **22**, 2132–2137.
Mappes, T., Achenbach, S. & Mohr, J. (2007). *Microel. Eng.* **84**, 1235–1240.
Meyer, P., Schulz, J., Hahn, L. & Saile, V. (2008). *Microsyst. Technol.* **14**, 1491–1497.
Pérennès, F., De Bona, F. & Pantenburg, F. J. (2001). *Nucl. Instrum. Method Phys. Res. A*, **467–468**, 1274–1278.
Romanato, F., Tormen, M., Businaro, L., Vaccari, L., Stomeo, T., Passaseo, A. & Di Fabrizio, E. (2004). *Microel. Eng.* **73–74**, 870–875.
Seward, T. P., Smith, C., Borrelli, N. F. & Allan, D. C. (1997). *J. Non-Cryst. Solids*, **222**, 407–414.
Soler-Illia, G. J. A. & Innocenzi, P. (2006). *Chem. Eur. J.* **12**, 4478–4494.
Van de Leest, R. E. (1995). *Appl. Surf. Sci.* **86**, 278–285.
Werst, D. W. & Vinokur, E. I. (2001). *J. Phys. Chem. B*, **105**, 1587–1593.